e-Navi

Available online at http://www.e-navigation.kr/
e-Navigation Journal

Original article

Numerical simulation of the flow field around a circular cylinder with racks

Tong ZHAO[a],Haihua LIN[b] , Hongyuan SUN[c], Bo JIAO[d], Chengmeng SUN[e], Bo GAO[f]

[a] Naval Architecture and Port Engineering College, Shandong Jiao Tong University, Weihai 264209, China, 940028744@qq.com

[b] Naval Architecture and Port Engineering College, Shandong Jiao Tong University, Weihai 264209, China, 222018@sdjtu.edu.cn

[c] Naval Architecture and Port Engineering College, Shandong Jiao Tong University, Weihai 264209, China, 216010@sdjtu.edu.cn

[d] Naval Architecture and Port Engineering College, Shandong Jiao Tong University, Weihai 264209, China, 200003@sdjtu.edu.cn

[e] Naval Architecture and Port Engineering College, Shandong Jiao Tong University, Weihai 264209, China, 222019@sdjtu.edu.cn

[f] Naval Architecture and Port Engineering College, Shandong Jiao Tong University, Weihai 264209, China, 216022@sdjtu.edu.cn

Abstract

The rack cylinder is an important part of the pile leg structure of the jack up platform. Because of its complex structure, the flow field around the rack cylinder is different from that around the ordinary cylinder, which brings difficulties to the research of the rack cylinder. In this paper, using CFD(Computational Fluid Dynamics) solved the flow field of chords with different rack height and rack width under different *KC* and *Re*, the characteristics of the flow field around the cylinder with rack are obtained. The results show that *Re*, *KC*, rack height and rack width all have different effects on the flow field. When Re and *KC* are constant, C_d will increase with the increase of rack height ratio, the change of C_d and C_l is not significant, while the change of C_d and C_l varies with *Re* when the chord structure is fixed.

Keywords: Cylinder, Rectangular rack, CFD

https://doi.org/10.52820/j.enavi.2023.21.001

1. Introduction

With the decreasing amount of energy on land, people have shifted the focus of energy extraction to the energy rich ocean. Various types of ocean platforms have emerged, among which self elevating platforms have been widely used due to their ability to achieve lifting. Due to the special marine environment, they are prone to damage. When seawater flows through structures on the ocean, such as offshore platform risers, alternating shedding vortices will appear behind them, causing damage to the structures Liu(2022a、2022b).

Scholars at home and abroad have carried out a lot of research on the phenomenon of flow around, from the initial two-dimensional cylindrical flow to the two-dimensional flow with different shapes. With the advancement of science and technology, they have begun to study more complex three-dimensional flow around different structures. Arum S. Mujumdar(1971, 1973) measured the eddy current shedding frequency of many cylinders with various geometric shapes, and found that the eddy current shedding frequency has little effect on the wake under a certain surface roughness. Phuocloc et al. (1985). solved the momentum equation by using the difference scheme, and verified the validity of the higher-order numerical scheme. Chaplin and Teigen (2003) carried out the cylindrical model experiment in the dragging pool. In the experiment, it was assumed that the ratio of *Re(Reynolds number)* to *Fr* was fixed, *Re*/*Fr(Froude)* = 2.79×10^5, and it was found that when *Fr* = 1, the total force coefficient reached the maximum value. YUE et al. (2011) analyzed the lift resistance of different shapes of cylinders at a fixed low *Re*, and found that it was consistent with the experimental results published by Strouhal number. Zhao et al. (2020) carried out numerical simulation of infinitely long cylinder with free liquid surface under the working conditions of *Fr* = 0.3 and *Re* = 4.2×10^4, and confirmed that the effect of free liquid on the cylinder is significant. POTTS D A et al. (1998, 2019) studied the flow field around cylinders with different cross-sectional shapes at low *Re*, and focused on the periodic variation characteristics of drag and lift, and found that there was obvious vortex-induced vibration in the wake. Sohankar et al. (1998) studied the flow around a two-dimensional square column, they found that strong vortex shedding occurs with the increase of the incidence angle under a certain range of incidence angles. Lin Zhijiang, Guo Jianting, Meng Xiaofeng (2020) and other scholars studied a single two-dimensional square column, the results showed that *Re* mainly affects the pulsating pressure, and each monitoring parameter changes greatly with the cross-section aspect ratio. Charles et al. (2010) studied the flow around a cylinder at subcritical *Re*, and carried out the simulation calculation of the flow around the cylinder using DES(Detached Eddy Simulation) method, and also compared the calculation results with the experimental results, and found that the position of the shed vortices is predicted very well by the finer time step. Catalano (2003) studied the feasibility and accuracy of LES(large eddy simulation). The results were compared with those obtained from steady and unsteady RANS (Reynolds-averaged Navier-Stokes) solutions and the available experimental data. The LES solutions are shown to be considerably more accurate than the RANS results. They captured correctly the delayed boundary layer separation and reduced drag coefficients consistent with experimental measurements after the drag crisis.Zhang Yizhao (2021) simulated the vortex-induced vibration of the cylinder when *KC(Keulegan–Carpenter number)*=25 and 50 in the oscillating flow. The results showed that the oscillating flow can excite the multi-modal motion of the cylinder, and the larger the KC number, the more obvious the multi-modal characteristics. Compared with the problem of flow around a single cylinder (1996, 2016), the problem of flow around a chord with a rack is much more complicated. Lin Haihua and Sun Chengmeng (2020) found some rules through simulating the flow field of the cylinder with racks(chord): when the direction of the incoming flow velocity and the rack are at an angle of 90°, the negative pressure area of the chord wake and the tail vortex area increase significantly, and C_l and C_d are also increases at the same time, and the surrounding flow field becomes more complex too. In recent years, Wu Yutao (2017) and other scholars have summarized the force and flow state of the flow around single, double cylinders and cylinder groups through the analysis of the flow around the cylinder, and proposed that the academic community should focus on the flow around the cylinder under more complex environmental conditions. Further research on marine risers, etc. Breuer (2000) created a three-dimensional model to study the flow field around riser, and compared the simulation results with the relevant literatures with

the same preconditions, and obtained consistent experimental results. There have been extensive studies on the flow around cylinders in the published literature, but there are relatively few studies on cylinders with complex racks, which are an important part of the self-elevating platform. Based on this, the flow field around cylinder with racks is considered and analyzed in this paper.

2. Numerical method

2.1 control equations

Assuming that the seawater is viscous and incompressible, the phenomenon of seawater flow around the cylinder with racks(chord) can be described by N-S equation. The N-S,Qu (2017) equation is:

$$\begin{cases} \dfrac{\partial u_i}{\partial x_i} = 0 \\ \dfrac{\partial u_i}{\partial t} + \dfrac{\partial}{\partial x_j}\left(u_i, u_j\right) = -\dfrac{1}{\rho}\dfrac{\partial p}{\partial x_j} + \dfrac{\partial}{\partial x_j}\left(v\dfrac{\partial u_i}{\partial x_j}\right) + f_i \end{cases} \quad (1)$$

where:

u_i and $u_j$is the velocity component;

ρ is pressure;

ν is the fluid kinematic viscosity coefficient;

f_i is the component of the external force;

ρ is the density;

t is time.

2.2 Turbulence model

The flow field around the cylinder with racks is in a turbulent state. For simulation and analysis, the SST K-ω model was selected. The SST model, Liu (2016), was modified from the standard model to solve the computational problem near the wall. Since the flow near the wall is not completely turbulent, simulating the flow process with the K-ε model would not be accurate. The K-ω model is necessary to simulate the flow near the wall, as the fluid in this region is bound and experiences tangential flow. The transport equations for turbulent kinetic energy K and specific dissipation rate ω in the SST model are expressed as follows:

$$\frac{D}{Dt}(\rho k) = \tau_{ij}\text{-}\beta^*\rho\omega k + \frac{\partial}{\partial x_j}\left((\mu + \sigma_k\mu_t)\frac{\partial k}{\partial x_j}\right) \quad (2)$$

$$\frac{D}{Dt}(\rho\omega) = \frac{\gamma}{\upsilon_t}\tau_{ij}\frac{\partial u_i}{\partial x_j}\text{-}\beta\rho\omega^2 + \frac{\partial}{\partial x_j}\left((\mu + \sigma_{\omega u_t})\frac{\partial \omega}{\partial x_j}\right)$$

$$+2(1 - F_1)\frac{\rho\sigma_{\omega 2}}{\omega}\frac{\partial k}{\partial x_j}\frac{\partial \omega}{\partial x_j} \quad (3)$$

For the meaning of specific parameters in the formula, please refer to Menter F R(1994).

3. Computational model

3.1 Geometric model of the cylinder with racks

The structure diagram of the cylinder with racks(chord) is shown in Figure 1, which are mainly composed of a cylinder and some racks. The rack height *H*, rack width *B*, and radius *R* are all marked in Figure 1.

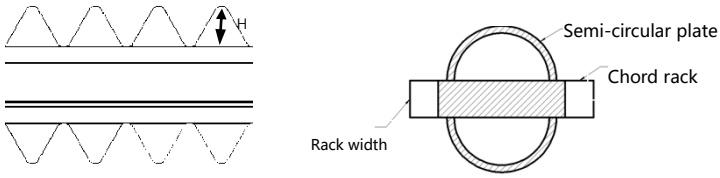

Figure 1: Geometric Model Diagram

3.2 Flow filed region and boundary conditons

The calculation region of the chord and boundary conditions are given in Figure 2. The total region is a rectangle, the incoming flow is from the left side. The detailed dimensions of the rectangular calculation region is showed in Figure 2, in which dimension D equals 2R.

The velocity inlet is employed for the left boundary, and the free outflow is employed for the right boundary. The symmetrical conditions are adopted for upper and lower boundaries, and the wall condition of free slip is used for the chord.

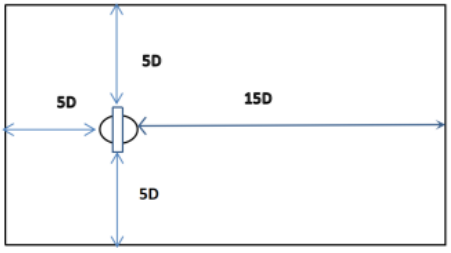

Figure 2: Flow Field Region and Boundary Conditions

3.3 Grid plot

In the near-wall treatment, 10 layers of boundary layers are set, and the mesh height of the first layer corresponds

to y^+≈1. Soft behavior is selected for grid size growth to make sure that the generated mesh is more tightly connected and the growth rate is set to 1.02. The grid is shown in Figure 3.

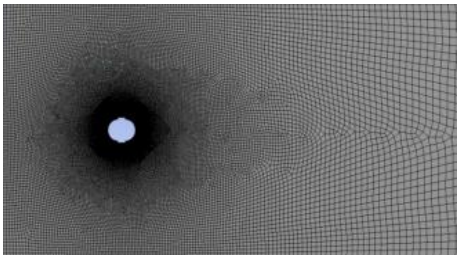

Figure 3: Grid Plot

4. Analysis conditions

When the fluid flows over the racked cylindrical surface, the chord is suffered the drag and lift force from the fluid. Since the racked cylinder tends to move forward under the action of the fluid, the drag on the chord is consistent with the direction of fluid flow, and the lift force is perpendicular to the flow direction. Various structural forms and various flow conditions are considered in this study. Five different rack height ratios of H/R are included and they are shown in table 1. And five different rack width ratios of B/R are discussed and they are showed in table 2.

Table 1: Different rack height ratios

H(mm)	R(mm)	（H/R）
5	95	0.053
15	95	0.158
25	95	0.263
35	95	0.368
45	95	0.474

Table 2: Different rack width ratios

B(mm)	R(mm)	B/R
44	95	0.463
54	95	0.568
64	95	0.675
74	95	0.780
84	95	0.884

Different *KC*s(*KC*=2, 4, 6, 8 10) are used in the analysis for considering the effect of oscillating incoming flow. *KC* is a dimensionless number and is related to the effect of the unsteady flow field on an object, such as wave. Expression of *KC* is as follows.

$$KC=\frac{VT}{L} \tag{4}$$

Where *V* is the amplitude of the velocity oscillation (if the object is oscillating, it is the amplitude of the velocity of the object) , *T* is the period of the oscillation, and *L* is the characteristic length of the object.

Different Res(3900, 5000, 6700, 7900, 9600) are used in the analysis for considering the effect of incoming velocity and flow state. Expression of *Re* is as follows.

$$Re=\frac{\rho v d}{\mu} \tag{5}$$

v, ρ and μ are the velocity, density and viscosity coefficient of the fluid respectively, and *d* is a characteristic length.

5. Analysis results

The analysis results of drag coefficient C_d, lift coefficient C_l, and variable quantity clouds are given under different analysis conditions.

5.1 C_l and C_d under different rack heights

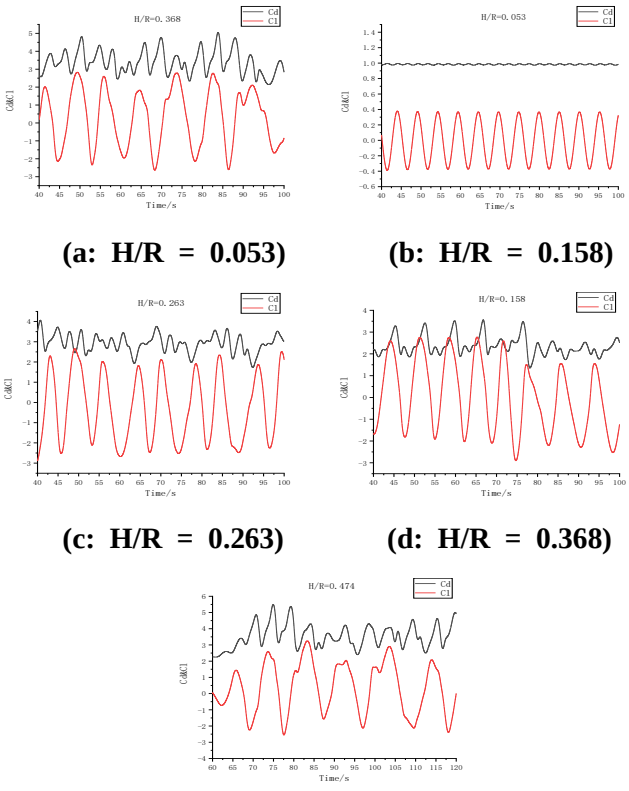

(a: H/R = 0.053) **(b: H/R = 0.158)**

(c: H/R = 0.263) **(d: H/R = 0.368)**

(e: H/R = 0.474)

Figure: 4 C_d and C_l Under Different H/R

The figures above show the time history of C_d and C_l at five ratios. Both C_d and C_l exhibit periodicity. As the chord rack height increases, C_d and the drag force on the chord also increase. This suggests that larger rack heights

result in greater resistance to the chord, and protruding racks can amplify the drag force on the structure. Furthermore, the C_l value fluctuates above or below zero, and the period of fluctuation increases with the ratio. This indicates that the time it takes for C_l to reach a stable change is longer with an increase in rack height. This is due to the rack's prominent shape, which causes boundary layer separation and generates periodic lift. The boundary layer separation point shifts with changes in the rack's shape. As the rack height increases, the distance between the separation points at both ends also increases. This results in an increase in the distance of fluid particle oscillation, leading to a longer oscillation period.

5.2 Fluid clouds under different rack heights

The velocity and vorticity clouds under different rack heights are given in below figures.

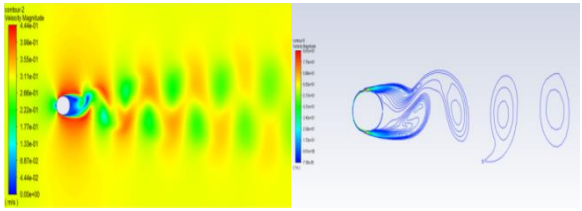

(a: H/R = 0.053)

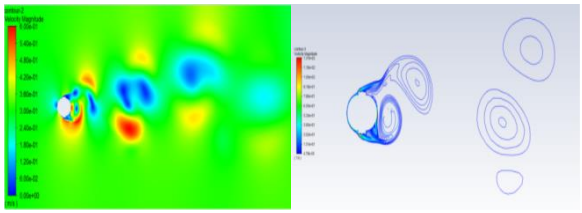

(b: H/R = 0.158)

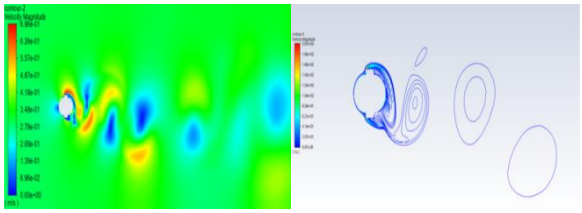

(c: H/R = 0.263)

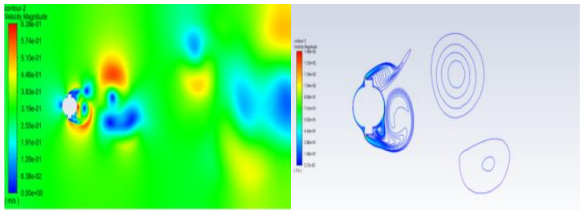

(d: H/R = 0.368)

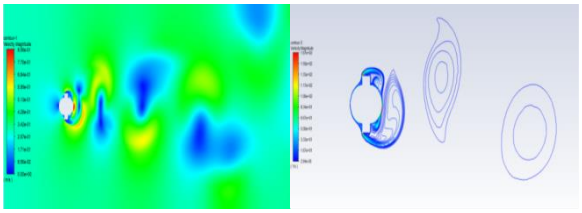

(e：H/R = 0.474)

Figure 5: Velocity and Vorticity Clouds Under Different H/R

It can be seen from the above figures that the maximum speed increases with the increase of the rack height ratio. Based on the fluid mechanics, the velocity of the incoming flow is reduced to zero as it moves along the wall of the chord meniscus to both sides. When it is reaching the corner where the meniscus meets the rack, the pressure is maximum, and the velocity changes abruptly at the corner of the rack near the direction of the incoming flow, the boundary layer separates obviously, the vertical distance between the two separated fluids increases, and the boundary layer on the chord surface changes from laminar flow to turbulence, the rear vortex becomes completely turbulent. With the increase of the rack-height ratio, the fluid blocked by the upper rack will flow down the chords and form a vortex, while the fluid blocked by the lower rack will flow in the opposite direction. The vortex falls off periodically according to a certain frequency. With the increase of the ratio of rack height, the fall-off vortex shape becomes more and more irregular.

5.3 C_l and C_d under different rack widths

The analysis results of drag coefficient C_d, lift coefficient C_l, and variable quantity clouds are given under different analysis conditions.

The C_l and C_d results are given in Figure 6, in which, b is rack width ratios of B/R.

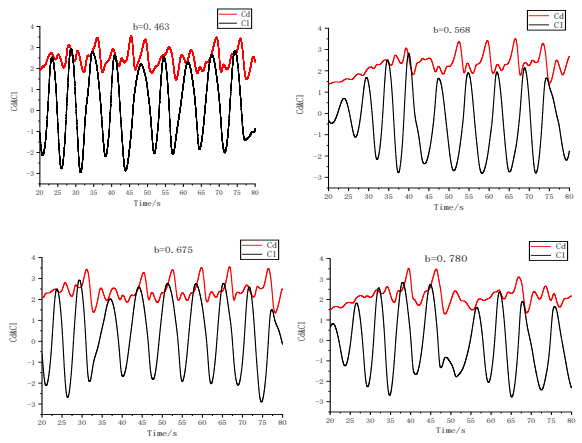

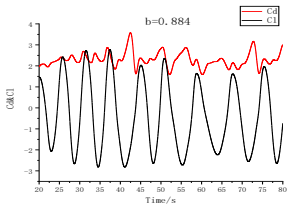

Figure 6: C_l and C_d Under Different B/R

It can be seen from the figures above that as B/R continues to increase, the mean value of C_d of the chord decreases first and then increases, while C_l also decreases first and then increases. This is because the length of the structure along the fluid direction increases when the rack width increases under one certain inflow conditions. Because of the viscous effect of the fluid, the drag force of the fluid on the structure increases. When the tooth width continues to increase, it means that the flow state of fluid along the rack width direction is relaxed, and the flow begins to ease, so the drag force of fluid on the structure starts to decrease. The same is true for lift.

5.4 Velocity clouds under different rack widths

Velocity contours under different rack width ratios are shown in Figure 7.

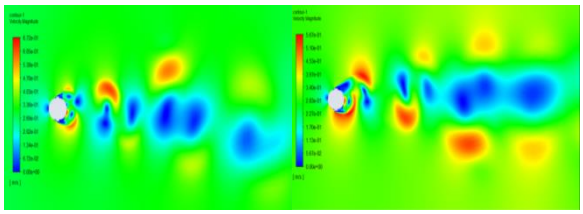

（b=0.463） (b=0.568)

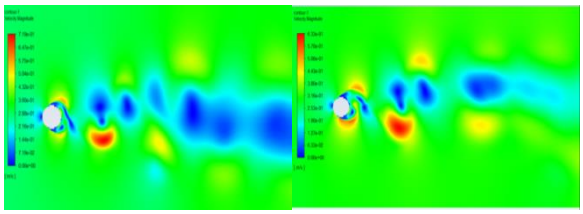

(b=0.675) (b=0.780)

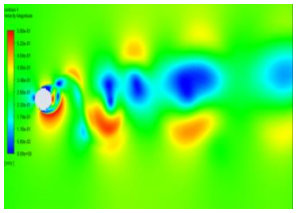

(b=0.884)

Figure 7 :Velocity Clouds Under Different b

From the velocity clouds above, it can be concluded that the front and back of the chord are low-velocity areas, and the pressure is relatively high. While high-velocity areas are formed on the upper and lower sides, and the pressure is relatively low. When b is from 0.463 to 0.568, the area of low-velocity area and high-velocity becomes to increase, which accelerates the vortex shedding. When b=0.675, while the high-speed area decreases, the low-speed area continues to increase, and the surrounding vortex shedding becomes more and more obvious. When b is from 0.780 to 0.884, the high-velocity area starts to increase again and the vortex falls off faster and faster.

5.5 Analysis results under different KCs

The following figures shows the time history of C_l and C_d under different *KCs*.

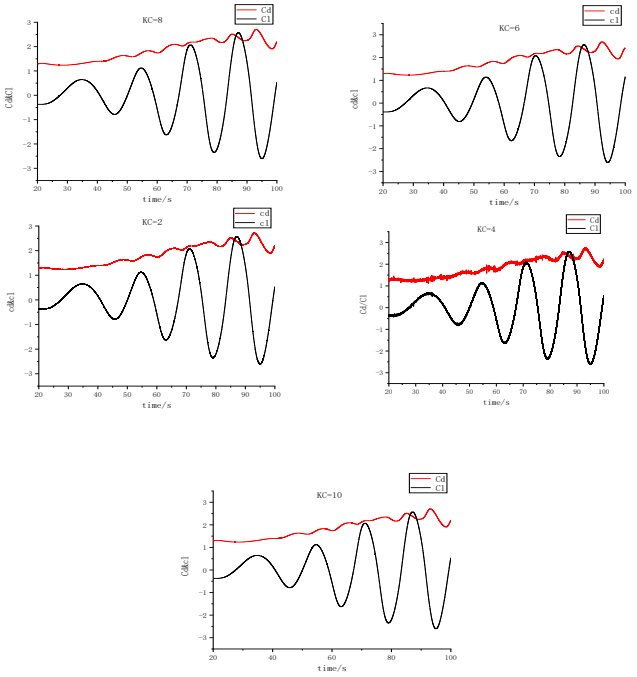

Figure 8: C_d and C_l Under Different *KCs*

It can be seen from the above figure 8 that when the *KC* values are 2, 4, 6, 8, and 10, the effect on the overall trend of the C_d and C_l curves is not obvious. This may be because the *KC* value is not large enough, the flow field oscillation is relatively small, and the influence on the flow field around the structure is also small. Therefore, the *KC* value can be further increased to observe its influence on the flow field around the structure.

5.6 Analysis results under different Res

Time history of C_d and C_l under different Res are shown in Figure 9.

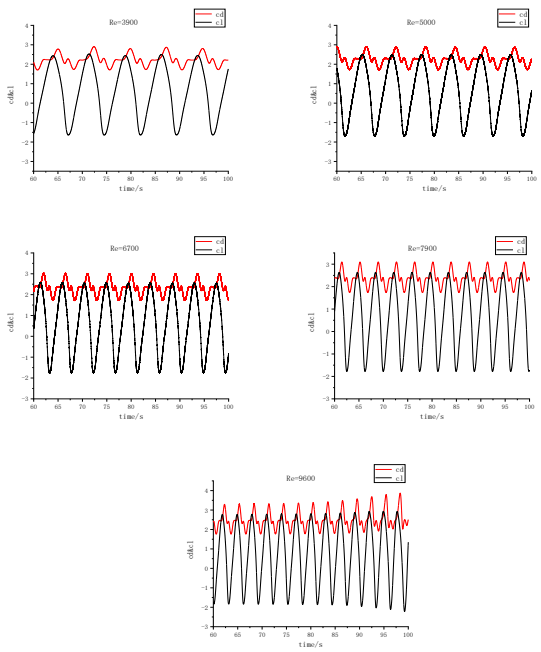

Figure 9: C_d and C_l Under Different *Res*

If the shape of the structure remains unchanged, as the inflow velocity increases, the Re value increases, the turbulence becomes more pronounced, and the boundary layer becomes thinner. Thus, the velocity gradient in the boundary layer becomes larger, and the drag force caused by the fluid viscosity increases. At the same time, due to the thinning of the boundary layer, the kinetic energy of the fluid at the upper and lower sides of the boundary layer separation area is larger, which will cause a large lateral oscillation force. In addition, when the incoming flow velocity increases, the kinetic energy of the whole flow field is larger, and the energy exchange rate of water quality in the flow field is accelerated, so the oscillation period of the drag force and lift force becomes shorter. Turbulent kinetic energy clouds under different *Res* are shown in Figure 10.

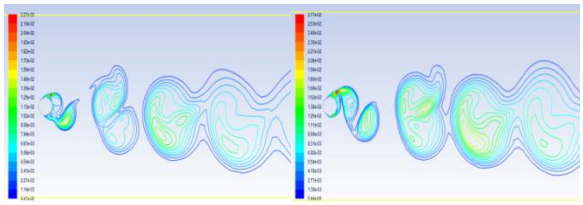

***Re*=3900** ***Re*=5000**

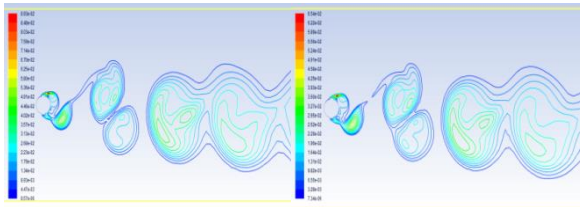

***Re*=6700** ***Re*=7900**

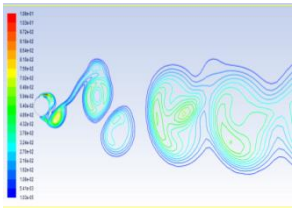

***Re*=9600**

Figure 10: Turbulent Kinetic Energy Under Different *Res*

It can be seen that with the increase of *Re*, the turbulent kinetic energy value becomes larger and larger similarly.

6. Conclusion

The numerical simulation of the flow field around a two-dimensional circular cylinder with racks is performed in this paper, and the following conclusions can be summarized.

(1) Rack height has a significant effect on fluid flow. The greater the rack height, the more the fluid flow is obstructed, the greater the C_d coefficient, the greater the disturbed area of the flow field, and the greater the turbulent kinetic energy and dynamic pressure.

(2) The influence of the rack width on the flow field is significant. Within a certain range of rack width ratios, vortex shedding accelerates as the rack width ratio increases. However, the opposite is true when the rack width ratio exceeds its critical value.

(3) Small changes in the low *KC* number have little effect on the C_l and C_d of the racked cylinder.

(4) The influence of *Re* on the flow field is also significant. The value and oscillation frequency of C_d will change with the change in *Re*. The larger the *Re*, the more significant the eddy current, the larger the vortex.

Funding: This research was funded by National Natural Science Foundation of China Youth Fund (grant number 51909148), ‘Climbing plan’ of Shandong Jiaotong University (grant number SDJTUC1802), and Doctoral Research Initiation Fund of Shandong Jiaotong University (grant number BS201901016 and BS2018001).

Conflicts of Interest: The authors declare no conflict of interest.

Acknowledgments: The authors would like to thank Yating Wang, Cui Liu, Qiaoyan Wang, Lufang Wang for their valuable work on this paper.

References

Mair, W. A., & Maull, D. J. (1971), Bluff bodies and vortex

shedding–a report on Euromech 17, *Journal of Fluid Mechanics*, 45(2), pp. 209-224.

Mujumdar, A. S., & Douglas, W. J. M. (1973), Vortex shedding from slender cylinders of various cross sections.

Loc, Ta, phuoc, et al,J,J. Fluid Mech, (1985),Numerical solution of the early stage of the unsteady viscous flow around a circular cylinder: a comparison with experimental visualization and measurements.

Chaplin, J. R., & Teigen, P. (2003), Steady flow past a vertical surface-piercing circular cylinder,*Journal of Fluids and Structures*, 18(3-4), pp. 271-285.

Yue, L., Zhang, Z. G., Feng, D. K., & Mudaliar, A. V. (2011), Investigation of the Flow and Heat Transfer around Cylinders at Low Re, In Advanced Materials Research Vol. 156, pp.

Zhao, W, Wan, D, & Zhao, S. (2020), CFD simulation of two-phase flows past a surface-piercing circular cylinder. I n ISOPE International Ocean and Polar Engineering Confe rence pp. ISOPE-I.

Potts, D. A., Binns, J. R., Marcollo, H., & Potts, A. E. (2 019), Hydrodynamics of towed vertical surface-piercing cyl inders. In International Conference on Offshore Mechanics and Arctic Engineering Vol. 58769, p. V001T01A024.

BOGRAD D D，GARRISON D H. (1998), Moment and heat transfer from cylinders in laminar cross-flow at $10^{-4}\leq$ Re≤200 J, *International Journal of Heat and Mass Transfe r*.

Sohankar, A., Norberg, C., & Davidson, L. (1998), Low-Reynolds-number flow around a square cylinder at incidence: study of blockage, onset of vortex shedding and outlet boundary condition, *International journal for numerical methods in fluids*, *26*(1), pp. 39-56.

Williamson, C. H. (1996), Vortex dynamics in the cylinder wake. Annual review of fluid mechanics, 28(1), pp. 477-5 39.

Duan Muyu & Wan Decheng. (2016), Large eddy simulatio n of 3D flow around a circular cylinder at Reno number 3900. Marine Engineering (06), pp. 11-20.

Lin Haihua & Sun Chengmeng. (2020), Analysis of the fl ow field around chords at different Reno numbers ,Procee dings of the thirty-one TH National Symposium on Hydro dynamics pp. 399-405.

Wu Yutao, Ren Huatang & Xia Jianxin. (2017) , Research progress and prospect of flow around a circular cylinder. Water Transport (02), pp. 19-26+56

Mockett, C., Perrin, R., Reimann, T., Braza, M., & Thiele, F. (2010), Analysis of detached-eddy simulation for the fl ow around a circular cylinder with reference to PIV data. Flow, turbulence and combustion, 85(2), pp. 167-180.

Breuer, M. (2000), A challenging test case for large eddy simulation: high Reynolds number circular cylinder flow. *I nternational journal of heat and fluid flow*,21(5), pp. 648-6 54.

Catalano, P., Wang, M., Iaccarino, G., & Moin, P. (2003), Numerical simulation of the flow around a circular cylind er at high Reynolds numbers. *International journal of heat and fluid flow*, 24(4), pp. 463-469.

Liu Zhijiang, Guo jianting, Meng Xiaofeng & Liu Haoran. (2020), CFD-based hydrodynamic simulation of flow arou nd square cylinder. *Ship Science and technology* (17), pp. 36-41.

Wang Kunpeng, Chi Qinghai & Zhang Yizhao. (2021), N umerical analysis of vortex-induced vibration of a cylinder in oscillating flow. Journal of Harbin Engineering Universit y (01), pp. 96-104.

Qu Xin Chen, Gao Yangyang, Liu Cai & Yang Kang. (2 017), Numerical simulation of three-dimensional flow arou nd a cylinder under different Reynolds numbers. Chinese Society of Ocean Engineering. (eds.) The 18th China Ocea n(Shore) Engineering Academic Proceedings of the Sympo sium (Part 1) (pp. 247-256). Ocean Press.

Liu Yue, Guan Xiaorong & Xu Cheng. (2016), Compariso n of the application of different SST modes in the simulat ion of flow around a slender body. Engineering Mechanics (11), pp. 240-248.

Menter, F. R. (1994), Two-equation eddy-viscosity turbulen ce models for engineering applications. *AIAA journal*, 32 (8), pp. 1598-1605.

Liu, M.M., Wang, H.C., Shao, F.F., Jin, X., Tang, G.Q., Yang, F. (2022), Numerical investigation on vortex-induced vibration of an elastically mounted circular cylinder with multiple control rods at low Reynolds number. Appl. Ocea n Res. 118, pp. 102987.

Liu, M.M., Wang, H.C., Shao, F.F., Jin, X., Tang, G.Q., Yang, F. (2022), Numerical investigation of local scour aro und a vibration pipeline under free surface wave condition. Ocean. Eng. 245, pp. 110556.

Received **04 September 2023**

1st Revised **30 November 2023**

2nd Revised **15 December 2023**

3rd Revised **23 December 2023**

Accepted **25 December 2023**